IEEE Access
Multidisciplinary | Rapid Review | Open Access Journal

Received March 14, 2020, accepted March 30, 2020, date of publication April 1, 2020, date of current version April 29, 2020.

Digital Object Identifier 10.1109/ACCESS.2020.2985012

5G Cellular and Fixed Satellite Service Spectrum Coexistence in C-Band

EVA LAGUNAS, (Senior Member, IEEE), CHRISTOS G. TSINOS, (Member, IEEE), SHREE KRISHNA SHARMA, (Senior Member, IEEE), AND SYMEON CHATZINOTAS, (Senior Member, IEEE)

Interdisciplinary Centre for Security, Reliability and Trust (SnT), University of Luxembourg, L-1855 Esch-Belval, Luxembourg

Corresponding author: Eva Lagunas (eva.lagunas@uni.lu)

This work was supported in part by the Luxembourg National Research Fund (FNR) and in part by the French Agence Nationale de la Recherche under the Bilateral CORE Project Spectral Efficient Receivers and Resource Allocation for Cognitive Satellite Communications (SIERRA).

ABSTRACT The C-Band (3.4 - 4.2 GHz) is a cornerstone for many satellite services including Fixed Satellite Service (FSS), in particular above 3.6 GHz. The large geographic coverage of C-band satellite beams represents a cost-effective communication solution, while its robustness to weather impairments makes C-band the most suitable band to guarantee high service availability. On the other hand, C-band has long been a top candidate for the deployment of 5G-cellular systems because it is a mid-band spectrum, blending the signal reach of lower bands with the capacity of higher bands. The potential assignment of C-band to the 5G cellular systems is seen as a threat by the satellite operators, who are concerned about the interference that the 5G-cellular system may cause to their services, potentially leading to service interruption and causing a serious economic impact. This paper presents the interference studies of 5G cellular systems operating in the below 6 GHz band in both the adjacent channel and co-channel scenarios. We present a detailed analysis for both 5G-celullar downlink and uplink, considering the impact of out-of-band emissions, potential Low-Noise Block (LNB) saturation at the FSS Earth station receiver and the consequences of the deployment of Active Antenna Systems (AAS) in the terrestrial Base Stations (BSs). The outcomes of this paper aim to shed some light to spectrum regulators and other related stakeholders regarding the impact of the future deployment of 5G-cellular systems in the FSS Earth station receivers operating in C-band. The paper also propose and evaluates potential techniques that can be applied to facilitate the coexistence of both systems, e.g. switching off critical emitters or backing-off their transmit power.

INDEX TERMS 5G cellular communication, Satellite communication, C-band, Interface management, Radio spectrum management.

I. INTRODUCTION

In contrast to the today's fourth generation (4G) of cellular networks, the upcoming fifth generation (5G) envisions to provide 1000 times increased capacity, 10-100 times higher data-rate, 10 times longer battery life, 5 times reduced end-to-end latency and to support 10-100 times higher number of connected devices [1]. However, there are still several challenges to be addressed in meeting these requirements, and many industries and academia are putting significant efforts towards enhancing spectral efficiency, system throughput, energy efficiency and connectivity in future wireless networks. One of the main limitations in meeting the capacity demands of future 5G and beyond networks is the unavailability of usable radio spectrum, i.e., spectrum scarcity caused due to the fragmentation of the spectrum and the current static frequency allocation policy [2], [3]. One possible approach to address this issue is to enable the sharing of the already allocated spectrum between different systems, leading to the concept of dynamic spectrum sharing [4]–[6]. However, the success of this technique in 5G systems heavily depends on the international and national regulatory bodies, as they are responsible to provide the new spectrum bands, to define the frequency coordination mechanisms, and operational guidelines for 5G deployment.

In the context of Europe, the main representatives of the digital technology industry have recently released the 5G spectrum policy recommendations [7], which is in

The associate editor coordinating the review of this manuscript and approving it for publication was Adnan Shahid.

accordance with the roadmap proposed by the Electronic Communications Committee (ECC) [8] and the 5G Infrastructure Public Private Partnership (5G PPP) vision [9]. The main priority bands identified for 5G systems in the context of Europe include 700 MHz (for wide area and indoor coverage including Internet of Things (IoT) applications), 3.4-3.8 GHz and 24.25-27.5 GHz (for 5G applications demanding very high data rates and capacity) [7]. Out of these, in this paper, we focus on the feasibility of using C-band (3.4-3.8 GHz) for 5G cellular deployment, which is currently being used in part by the Fixed Satellite Services (FSS) systems.

The 3.4-3.8 GHz band is already harmonized for mobile networks and is considered essential for 5G deployment, providing unique opportunity for early and wide-scale 5G deployment (it consists of up to 400 MHz of continuous spectrum enabling wide channel bandwidth). Given the bandwidth availability and the considerable range, frequencies below 6 GHz will most probably be used in the initial stage of 5G technology implementation, especially in Europe and America. However, C-band is widely used for satellite communications because of its wide geographic coverage area and robustness to different propagation conditions. While C-band spectrum has been traditionally reserved exclusively for satellite use, the regulatory bodies are in favor of allocating a portion of C-band to terrestrial broadband operators for the upcoming deployment of 5G. This has triggered some discussion between the satellite operators, the terrestrial mobile operators and the spectrum regulatory authorities in order to understand the implications of the C-band allocation [10]. In general, there is a clear agreement on the fact that the C-band should be carefully assigned to new 5G systems so as to ensure the continuity of vital satellite communication services.

One of the important aspects discussed during the 2019 World Radiocommunication Conference (WRC-19), held in November 2019 in Egypt, was the future 5G spectrum allocation [11], [12]. To adequately support the claims made in the WRC-19, different countries have internally run interference studies to better understand the potential implications of 5G co-sharing the satellite C and K band spectrum [13]–[16]. However, these studies have been tailored to particular country needs and scenarios of local interest. The academic community has also partially studied the impact of international mobile telecommunication (IMT) deployment into these bands. The authors in [17] presented results from an experimental campaign focusing on satellite Very Small Aperture Terminals (VSAT), whose location may not be known and that represents an important class of FSS terminals worldwide. In [18], a preliminary spectrum-sharing study was presented to evaluate the feasibility of coexistence between 5G and other existing services in the 28-GHz band. Similarly, sharing studies of 5G cellular and GSO–NGSO networks in the 28 GHz band in adjacent channel and co-channel scenarios were recently presented in [19]. On the other hand, spectrum co-existence and intelligent radio resource management have been studied in [6], [20], [21] with the main focus being the K/Ka band scenario. However, these studies provide a simple system level abstraction by analyzing the interference impact at the Signal-to-Interference Noise Ratio (SINR) level.

The protection of the existing satellite systems operating in the C-band is crucial while allocating C-band frequencies to the upcoming 5G deployment, and to accomplish this, suitable spectrum sharing mechanisms need to be investigated in the scenarios where satellite systems receive harmful interference from the terrestrial systems. In this regard, this paper aims to analyze the feasibility of utilizing either the whole 3.4-3.8 GHz band or a portion of this spectrum for 5G mobile services, without affecting the operation of existing FSS systems deployed within the same geographical area. In particular, we address and analyze the spectrum-based challenges and opportunities related to the 5G-satellite coexistence in C-band. In particular, a detailed interference study is carried out in order to define under which conditions which parts of the spectrum are usable in which geographical area. The study analyzes the harmful effects of the Block Edge Mask (BEM) and the resulting Out-Of-Band (OOB) emissions, the mitigation effect of including a received filter in the satellite terminals, the possible Low-Noise Block (LNB) saturation caused by the 5G interference and, last but not least, the impact of the deployment of Active Antenna Systems (AAS) in the 5G cellular base stations. The outcomes of the study provide insights on the appropriate conditions under which the use of C-band by the 5G mobile operators does not harm the satellite receivers operating in the C-band. In addition, for the 5G downlink scenario, we propose and analyze two interference mitigation strategies, one based on the complete switch-off of critical 5G BSs and another less radical than the previous one, which is based on power back-off applied to the 5G BSs. All the aforementioned analysis are carried out through numerical simulations using realistic system parameters.

This paper is organized as follows. Section II presents the system model for the 5G downlink in coexistence with the C-band satellite receivers, and introduces the corresponding signal and interference model as well. The 5G downlink analysis and supporting results based on numerical data are provided in Section III. Section IV provides the description of the 5G uplink scenario and Section V presents the numerical results for the 5G uplink case. Finally, Section VI concludes the paper.

II. 5G DOWNLINK SCENARIO

In this paper, we consider the coexistence scenario of FSS downlink (reception on earth) and the envisioned 5G cellular system. It is assumed that the 5G system utilizes Time Division Duplex (TDD) mode of operation in the C-band for the downlink and uplink with the perfect TDD synchronization between different operators networks, i.e. all BSs transmit/receive at the same time. In this section, we focus on the 5G cellular C-band downlink scenario, while Section III will elaborate on the 5G cellular C-band uplink scenario.

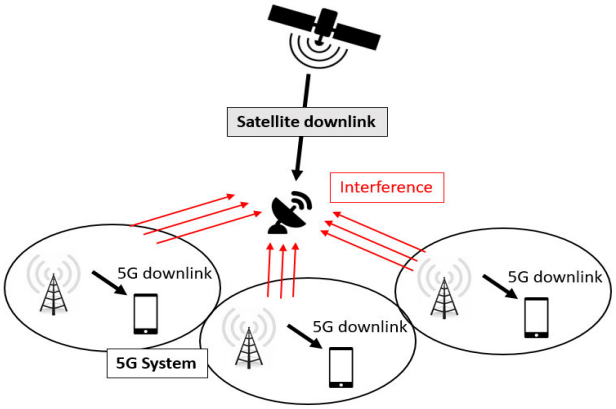

FIGURE 1. Scheme of the 5G cellular downlink scenario.

In the 5G downlink coexistence scenario, FSS Earth stations may receive harmful interference from the 5G cellular BSs, which are assumed to be omnidirectional (worst case). The deployment of Active Antenna Systems (AAS) in the 5G BSs is considered in Section III-E. The scenario of 5G cellular downlink interfering with the satellite receivers due to the C-band spectrum sharing is illustrated in Fig. 1. In particular, we assume M 5G BSs providing coverage to a specific area. Somewhere in the middle of such area, there is a FSS Earth station receiver operating between 3.625 GHz and 3.800 GHz, which is being interfered by the 5G downlink transmission.

A. 5G SYSTEM MODEL

The specifications related to the considered 5G downlink system is taken from the Table 4 of International Telecommunication Union (ITU) Report ITU-R M.2292 [22], which specifies the deployment-related parameters for bands between 3 and 6 GHz. In particular, we focus on the "Macro-Sub-Urban" case and take the worst Effective Isotropic Radiated Power (EIRP) given by EIRP = 61 dBm/5 MHz. Note that ITU-R M.2292 provides the characteristics of terrestrial IMT-Advanced systems. Although some formats and processes will be re-utilized for IMT-2020, ITU is currently working on an updated document for IMT-2020, which is expected to be finalized during 2020 [23]. In our analysis, and again with the aim of capturing the worst case, we choose the modeling of omnidirectional antennas for the 5G BSs. After testing different BS antenna height values, we fix it to 25 meters, assuming this as one of the worst reasonable heights (worst because it is high enough to "see" the FSS Earth station receiver from a far away distance).

In the below 6 GHz frequencies, the bandwidth required to support 5G requirements in terms of capacity and latency is in the order of 100 MHz [24]. In this paper, we provide results for two types of frequency allocations for the terrestrial operators, which are described in Table 1, and illustrated in Fig. 2. Note that both Table 1 and Fig. 2 provide a sample frequency assignment for 3 terrestrial operators (Operator 2 in the first spectrum block, Operator 1 in the second spectrum block and Operator 3 in the third spectrum block). Each operator is assumed to operate in a number of BSs sites, i.e. one BS site can be equipped with different equipment belonging to different operators.

TABLE 1. Considered spectrum allocation for the 5G cellular downlink.

	Option 100 MHz	Option 70 MHz
Operator 1	3400 – 3500 MHz	3410 – 3480 MHz
Operator 2	3500 – 3600 MHz	3480 – 3550 MHz
Operator 3	3600 – 3700 MHz	3550 – 3620 MHz

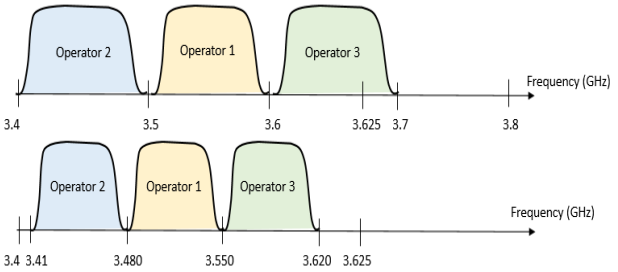

FIGURE 2. Frequency assignment for 5G downlink: (top) Option 100 MHz, (bottom) Option 70 MHz.

B. INTERFERENCE MODEL

Regarding the interference power calculation at the FSS Earth station receiver, the propagation losses are modeled according to ITU-R recommendation ITU-R 452.16 [25]. In particular, the propagation losses consist of the free space path loss and the diffraction loss. The free space path loss [dB] is calculated by using the following equation,

$$L_{\text{FSPL}} = 20 \cdot \log_{10}(D) + 20 \cdot \log_{10}(f_c) + 32.45, \quad (1)$$

where distance D is the propagation distance in Km and f_c is the carrier frequency is in MHz. The diffraction loss L_{diff} is computed by following the model proposed in Section 4.2 of ITU-R P.452-16, which essentially models the so-called knife-edgde diffraction loss, considering the Earth curvature, the actual terrain profile and antenna heights. In particular, the diffraction loss is calculated by the combination of a method based on the Bullington construction and spherical-Earth diffraction. We note that the model does not model clutter and polarization. Although including these two aspects may provide considerable benefit in terms of protection from interference, we opted to keep the model general without imposing any assumption on the surrounding environment of the antennas and transmit polarization. Therefore, the results obtained in this paper can be considered a worst-case scenario with respect to the level of received interference.

Finally, the interference power received at the FSS Earth station receiver can be expressed as follows,

$$P_{\text{int}} = \text{EIRP} - L_{\text{FSPL}} - L_{\text{diff}} + G_{\text{RX}} - G_{\text{filter}} \ [\text{dBW}], \quad (2)$$

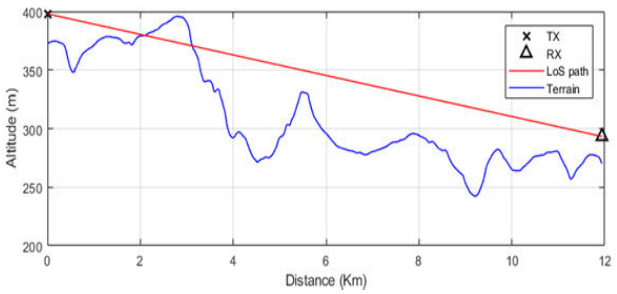

FIGURE 3. Example of propagation path used for the interference modelling.

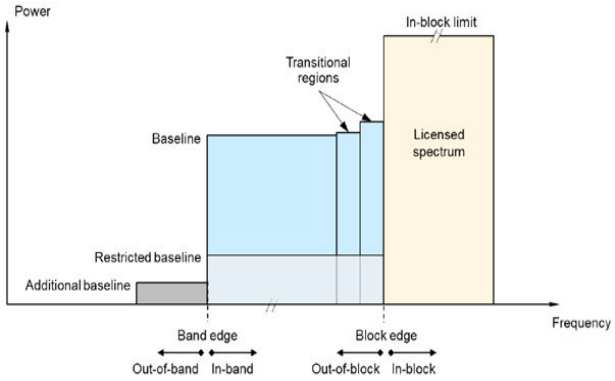

FIGURE 4. Illustration of the OOB emissions as per ECC report 281.

where G_{RX} denotes the antenna gain of the FSS Earth station receiver and G_{filter} denotes the rejection gain of the FSS Earth station receiver filter. All components in (2) are in decibel units. In the context of this study, we have used true terrain data to accurately account for the diffraction loss [26]. An example of true terrain profile between a given transmit location and a given receiver location is shown on Fig. 3.

C. OOB MODEL

To model the OOB emissions of the 5G downlink transmission, we follow the recommendations provided in ECC report 281 [27]. In particular, we model the transitional and baseline frequency regions as detailed in Fig. 2 and Fig. 4.

D. FSS EARTH STATION RECEIVER MODEL

The FSS Earth station receiver antenna gain G_{RX} is modelled according to ITU-R S.465-6 (01/2010) [28], which takes into account the dish diameters as well as the off-boresight angle. The FSS dish antenna height is fixed to 10 meters, assuming this to be a reasonable average height for FSS systems.

The noise level N_0 corresponding to the considered bandwidth is calculated using the well-known total thermal noise power formula given by $N_0 = K \cdot T \cdot B$, where K is the Boltzmann's constant having the value of $1.38 \cdot 10^{-23}$ J/K, $T = 110°$ K is the receiver noise temperature comprising of $70°$ K room temperature [29] plus antenna noise temperature of $40°$ K, and B is the bandwidth of operation. In general,

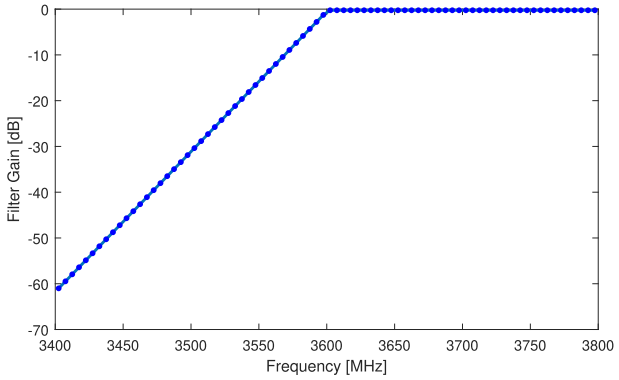

FIGURE 5. FSS Earth station receiver filter response.

the antenna temperature depends on the elevation of the antenna. We have used $40°$ K based on the specifications of the real antenna structures [30]. By following the above formula, the calculated noise levels N_0 are -141.20 dBW for $B = 5$ MHz, and -128.19 dBW for $B = 100$ MHz.

Finally, for the 5G downlink interference evaluation, we consider the following 3 types of FSS Earth station receiver antennas:

- **Antenna type 1:** Antenna with 12 m diameter, which points towards south with 33 degrees of elevation and 181 degrees azimuth.
- **Antenna type 2:** Antenna with 4.8 m diameter, which points towards west with 10 degrees elevation and 246 degrees azimuth.
- **Antenna type 3:** Antenna with 4.8 m diameter, which points towards east with 10 degrees elevation and 113 degrees azimuth.

We model the FSS Earth station receiver filter G_{filter} as a square root raised cosine (SRRC), which is depicted in Fig. 5 for the band of interest (3400-3800 MHz). Clearly, the band-pass of the filter is 3.625-4.2 GHz, assuming that the FSS downlink operations are confined to these frequencies.

The saturation point of the LNB is also important to respect. When too much RF power enters the LNB, the LNB saturates. In this paper, we use the 1 dB compression point of 2 dBm, which is defined as the RF input power required to cause the conversion loss to increase by 1 dB with respect to the theoretical linear response. This compression point is the maximum recommended RF input power to the LNB. As an example, assuming a general typical 65 dB LNB gain (for the antennas specified above), the maximum tolerable input power to the LNB becomes 2dBm-65dB $= -63$dBm. It should be noted that this value does not consider any protection margin and this margin needs to be defined.

A summary of the key system model parameters is prvided in Table 3.

III. 5G DOWNLINK RESULTS

In this section, simulation results obtained for the 5G downlink scenario are provided. We divided this section into two

TABLE 2. Model of the OOB emissions as per ECC report 281 [27].

BEM element	Freq. Range	Non-AAS EIRP limit dBm/(5MHz) per antenna	AAS TRP limit dBm/(5MHz) per cell
Transitional Region	-5 to 0 offset from lower block edge; 0 to 5 MHz offset from upper block edge	Min(PMax-40,21) [3]	Min(PMax′-40,16) [4]
Transitional Region	-10 to -5 offset from lower block edge; 5 to 10 MHz offset from upper block edge	Min(PMax-43,15) [3]	Min(PMax′-43,12) [4]
Baseline	Below -10 offset from lower block edge; Above 10 MHz offset from upper block edge. Within 3400-3800 MHz.	Min(PMax-43,13) [3]	Min(PMax′-43,1) [4]

[1]PMax is the maximum mean carrier power in dBm for the BS measured as EIRP per carrier interpreted as per antenna
[2]PMax′ is the maximum mean carrier power in dBm for the BS measured as TRP per carrier in a given cell

TABLE 3. System Model Parameters.

5G Downlink	
EIRP	61 dBm/5MHz
Number of BS (M)	1135
BS Antenna Height	25 meters
BS - satellite receiver distance	59 - 245 meters
Number of operators	3
Satellite System	
Rx Band	3.625 - 4.2 GHz
Receiver Noise Temp. (T)	110°K
Noise Power at 5 MHz (N_0)	-141.20 dBW
Interference Margin (I/N_0)	10 dB
Interference Threshold	-151.20 dBW
Antenna	Type 1: ∅12m, 33° elev., 181° azm. Type 2: ∅4.8m, 10° elev., 246° azm. Type 3: ∅4.8m, 10° elev., 113° azm.
Max. antenna gain	65 dB
LNB 1dB saturation point	2 dBm

main parts: (1) Individual interference impact study, where we analyze the effect of individual BS transmission into the FSS Earth station receiver, and (2) the aggregated interference impact, assuming the aggregation of multiple BS transmitting simultaneously.

In both cases, we assume 3 potential mobile operators which are assigned a maximum of 100 MHz non-overlapping spectrum block each, as explained in Section II-A. It should be noted that while considering the option of 100 MHz allocation for three operators (from 3400-3700 MHz), there arises the overlapping of upper part of the spectrum with that of the FSS system since the satellite system is operating in the band 3.625-4.2 GHz. In the situations where the received interference at the FSS Earth station receiver exceeds the tolerable interference threshold, different interference mitigation strategies such as switching off nearby BSs (exclusion zone) or power control (power back-off) towards the FSS Earth station receiver's location are investigated.

For evaluating the effect of individual and aggregated interference at the satellite receiver, the interference protection criteria of I/N $= -10$ dB is considered [31]. By considering both the noise levels calculated in Section II-D and the interference protection criteria of I/N $= -10$ dB, the interference threshold at the receiver antenna becomes: (i) -146.3871 dBW for $B = 5$ MHz, and (ii) -133.3748 dBW for $B = 100$ MHz.

A. INDIVIDUAL INTERFERENCE IMPACT

In this section, we evaluate the impact of individual BS transmission. In particular, we do not assume any predefined spectrum allocation for the 5G system. Instead, we assume that each BS can transmit in any 5 MHz frequency chunk available between $3.4 - 3.8$ GHz. The distribution of cellular BS significantly depends on coverage and capacity constraints, which at the same time are dependent on socioeconomic, demographic, and geographic variables. For the sake of simplicity, in this paper, we assume M $= 1135$ BSs uniformly and randomly distributed in the surrounding area of the satellite receiver, with a resulting separation distance between BS and FSS Earth station receiver ranging from 245 meters to 58.7 kilometers. Additional information about spatial BS distribution methods can be found in [32].

1) IMPACT OF OOB EMISSIONS

We study first of all the OOB emissions impact. The OOB emissions are residual low power transmission which can be seen as leakage to adjacent bands. Since these are low power transmissions, we expect not to have a huge impact on the satellite receiver. This is confirmed by the results shown in Table 4, where the number and percentage of BS generating interference levels at the satellite receiver above the interference threshold are detailed, for the different satellite antenna types described in Section II-D. It can be observed that a very low number of BSs generate harmful OOB emissions, accounting for ∼4-5% of the total number of BSs. Fig. 6 depicts the location of all the critical BS for the antenna type 2, which is the antenna giving higher number of critical BSs, and it can be concluded that BSs located at close vicinity of the satellite receiver, i.e. ∼14 Km, can perturb the satellite receiver operation, even when they are not aligned with the satellite antenna pointing. Note that the deployment of the filter in the satellite receiver (see Section II-D) has no mitigation effect on the OOB emissions, which fall directly into the spectrum assigned to the FSS Earth station receiver in any case.

TABLE 4. Impact of OOB for the 5G cellular downlink.

	Antenna type 1		Antenna type 2		Antenna type 3	
Operator	Number of BS whose OOB emissions generate interference	Percentage of BS whose OOB emissions generate interference	Number of BS whose OOB emissions generate interference	Percentage of BS whose OOB emissions generate interference	Number of BS whose OOB emissions generate interference	Percentage of BS whose OOB emissions generate interference
1	19	4.22%	21	4.67%	19	4.22%
2	15	4.05%	18	4.87%	15	4.05%
3	14	4.44%	17	5.40%	14	4.44%
Total	48	4.23%	56	4.93%	38	4.23%

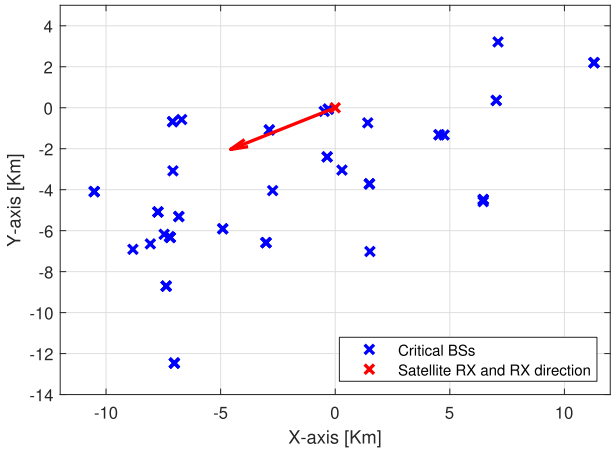

FIGURE 6. Location of BSs whose OOB generate harmful interference assuming antenna type 2.

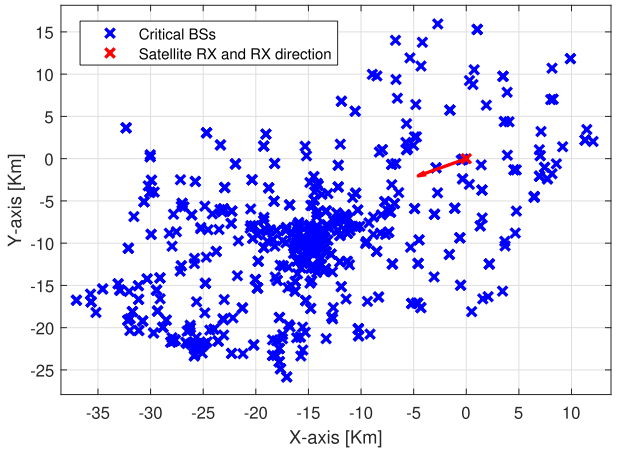

FIGURE 7. Location of BSs whose co-channel transmission generate harmful interference assuming antenna type 2.

2) IMPACT OF CO-CHANNEL INTERFERENCE ON THE FSS EARTH STATION RECEIVER LNB SATURATION

Next, we consider the maximum interference that a BS can cause to the FSS Earth station receiver location assuming the individual transmission of each BS of EIRP $=$ 61 dBm/5 MHz (ominidirectional). Again, we analyze any 5 MHz frequency chunk available between $3.4 - 3.8$ GHz. Therefore, we expect strong co-channel interference particularly for the band assigned to the satellite receiver, i.e. 3.625-4.2 GHz. The critical BSs are computed based on whether their individual interference levels received at the FSS Earth station receiver antenna exceed the defined interference threshold, and the worst-case scenario is considered by taking the maximum of the interference values over all the co-utilized frequency chunks while finding these critical BSs.

Under these assumptions and considering the same distribution of $M = 1135$ BSs in the surrounding area of the FSS Earth station receiver as before, we obtain the results summarized in Table 5. It can be observed that the results show a significant increase of the interference with respect to the OOB emissions only case presented in Section III-A.1, going from ∼4-5% up to ∼45% for antenna types 1 and 3, and up to ∼63% for antenna type 2. Therefore, even restricting the satellite service to the 3.625-3.8 GHz band and the deployment of a band-pass filter, the interference is still significant.

Focusing on antenna type 2, Fig. 7 shows the location of all the critical BSs. It can be observed that the satellite receiver antenna pointing plays an important role. In particular, it can be observed that BSs located at a distance farther than ∼16 Km of the satellite receiver do not cause problems if they are not located closer to the satellite receiver antenna pointing, while this minimum distance increases to ∼41 Km when the BS locations are aligned with the satellite antenna pointing.

B. AGGREGATED INTERFERENCE IMPACT

In this section, we focus on the analysis of aggregated interference, where aggregation happens across BSs of the same operator. Therefore, the spectrum allocation options described in Table 1, and illustrated in Fig. 2, become relevant. Note that we consider FSS/5G spectrum overlap for the 100 MHz block assignment; and FSS/5G non-overlapping for the 70 MHz block assignment.

To compute the OOB emissions for blocks of 70 MHz or 100 MHz, the guidelines of ECC report 281 were used as described in Section II-C. For any of the both considered allocation options (either 70 MHz or 100 MHz) we compute

TABLE 5. Impact of co-channel interference for the 5G cellular downlink.

	Antenna type 1		Antenna type 2		Antenna type 3	
Operator	Number of BS whose OOB emissions generate interference	Percentage of BS whose OOB emissions generate interference	Number of BS whose OOB emissions generate interference	Percentage of BS whose OOB emissions generate interference	Number of BS whose OOB emissions generate interference	Percentage of BS whose OOB emissions generate interference
1	203	45.11%	274	60.89%	195	43.33%
2	173	46.76%	236	63.78%	166	44.87%
3	141	44.76%	203	64.44%	134	42.54%
Total	517	45.55%	713	62.82%	495	43.61%

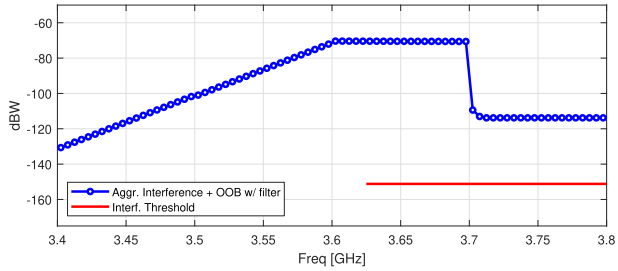

FIGURE 8. Resulting aggregated interference levels assuming antenna type 2 and the 100 MHz spectrum allocation option.

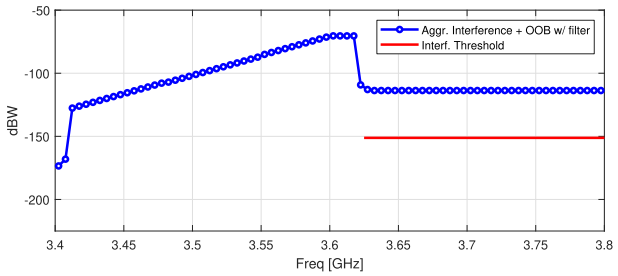

FIGURE 9. Resulting aggregated interference levels assuming antenna type 2 and the 70 MHz spectrum allocation option.

the OOB with the EIRP of a single BS operating at 5MHz frequency chunk (i.e., EIRP of 61 dBm). Next, we add the OOB emissions of all BSs operating on that spectrum block. The final OOB emissions impact is obtained by aggregating the OOB of all three operators.

In this section, we focus on the FSS Earth station receiver antenna type 2, which is shown to provide the worst antenna pointing in terms of received interference. First, we provide the results assuming FSS/5G spectrum overlap, i.e. the 100 MHz spectrum allocation option. Fig. 8 shows the resulting aggregated interference and compares with the FSS Earth station receiver interference threshold. It can be observed that operator 3 operating between 3.6-3.7 GHz is causing harmful interference to the FSS Earth station receiver, as its block appears to be above the threshold. Also, the OOB aggregation of all 3 operators appears to be above the threshold within the band 3.7-3.8 GHz.

Next, we evaluate the results assuming no FSS/5G spectrum overlap, i.e. the 70 MHz spectrum allocation option. Fig. 9 illustrates the resulting aggregated interference over the 3.4-3.8 GHz band. It can be observed that there is harmful interference at the satellite receiver caused by the OOB aggregation, as the blue line crosses the red threshold in the 3.625-3.8 GHz. Clearly, the non-overlapping 5G/FSS scenario can reduce the interference considerably.

1) SWITCHING-OFF CRITICAL BS STRATEGY

In order to reduce the interference, we implement a switching-off strategy, where the BSs are switched off starting from the one causing higher interference. For this particular scenario, we find out that 332 out of $M = 1135$ BSs need to be switched-off in order to decrease the aggregated interference (25 belonging to operator 1, 18 belonging to operator 2 and 289 belonging to operator 3). The final result is illustrated in Fig. 10. In particular, 29.25% of the total BSs need to be switched-off.

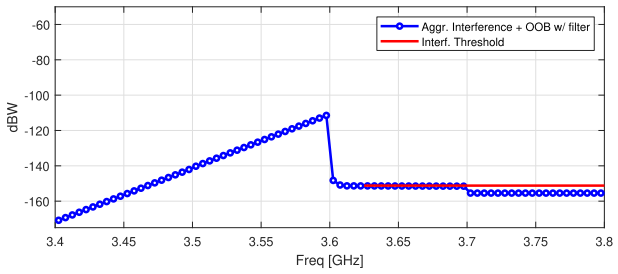

FIGURE 10. Resulting aggregated interference levels assuming antenna type 2 and the 100 MHz spectrum allocation option after switching off critical BSs.

Now we focus on the no FSS/5G spectrum overlap scenario, i.e. the 70 MHz spectrum allocation option. We perform the same exercises as before, which consists of switching off BSs one by one, starting from the one producing the highest interference, until the contribution of the aggregated active BSs is below the threshold. We find out that 56 out of $M = 1135$ BSs need to be switched-off in order to decrease the aggregated interference (21 belonging to operator 1, 18 belonging to operator 2 and 17 belonging to operator 3), which corresponds to a ∼5% of the total. Most importantly, the switching-off strategy for the 70 MHz spectrum allocation

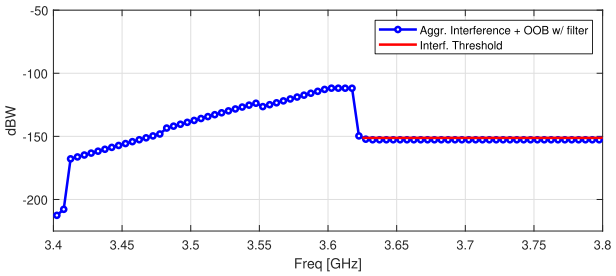

FIGURE 11. Resulting aggregated interference levels assuming antenna type 2 and the 70 MHz spectrum allocation option after switching off critical BSs.

is fair among operators, as approximately the same number of BSs needs to be switched off for each operator. The level of interference achieved with the switching-off strategy is depicted in Fig. 11.

C. AGGREGATED INTERFERENCE IMPACT ON LNB SATURATION

In this section, we focus on the 70 MHz spectrum allocation (see Table 1) which has been shown to be the most promising and less intrusive 5G spectrum allocation according to Section III-B. The LNB assumptions are detailed in Section II-D. We provide results for two different margin criteria to protect the satellite desired signal received at the LNB: (1) A conservative margin fixed to 25 dB, and (2) A more realistic margin fixed to 10 dB, according to robust LNB models available in he market [33].

1) RESULTS WITH LNB MARGIN OF 25 dB

The LNB interference saturation threshold is given by the maximum tolerable input power (i.e. −63 dBm) minus the margin, which in this case gives a threshold of −88 dBm (or equivalently −118 dBW). Note that this limit applies to the overall 3.4-3.8 GHz band.

We sum up the aggregated interference over the overall 3.4-3.8 GHz band, which is illustrated in blue in Fig. 9, and the total interference is equal to −62.15 dBW, which is definitely above the LNB saturation threshold. As a consequence, some kind of interference mitigation strategy has to be applied.

a: SWITCHING-OFF CRITICAL BS STRATEGY

Next, we consider the switching-off strategy, where certain critical BSs are switched off to meet the LNB threshold. Again, we switch off BSs starting from the worst one in terms of interference, until the LNB threshold is met. The results are summarized in Table 6. In particular, 160 BSs need to be switched off for operator 3, while the number reduces to 28 and 14, respectively for Operator 1 and Operator 3, which are located further apart from the FSS Earth station receiver in frequency domain. The total of BSs that need to be switched off in order not to saturate the LNB is 17.8%, and its location on the map are provided in Figure 12. As expected, the most harmful BSs are located in close vicinity to the FSS Earth station receiver.

TABLE 6. Switch-Off strategy results to avoid the LNB saturation (margin 25 dB).

Operator	Number of BS switched off	Percentage of BS switched off
1	28	6.22%
2	14	3.78%
3	160	50.79%
Total	202	17.8%

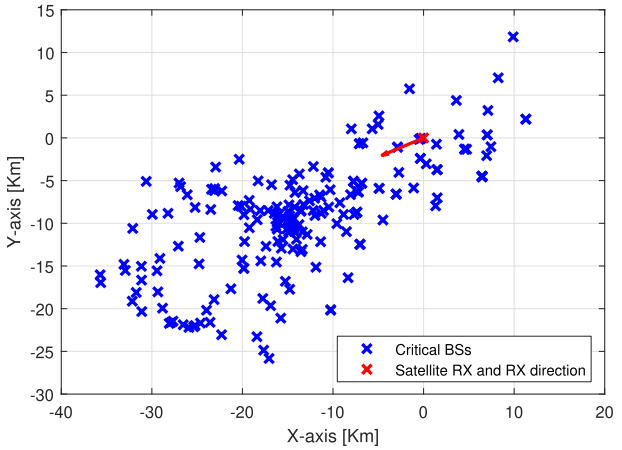

FIGURE 12. Location of BSs required to be switched off in order to not saturate the satellite LNB receiver assuming antenna type 2 and margin of 25 dB.

b: BS POWER BACK-OFF STRATEGY

Finally, we evaluate an alternative solution based on a power back-off strategy, where instead of completely switching off certain BSs, we reduce their transmitted power so as to meet the LNB threshold. However, there is no clear approach on how to define which BSs need to back-off, as multiple BSs operating across the whole band affect the LNB saturation. Therefore, it is very challenging to optimally establish: (1) the optimal number of BS within each back-off level, and (2) the optimal back-off levels. As a consequence, in this Section, we show some results based on a simple heuristic solution, which is explained in the next paragraph. We propose to cluster the BSs into different groups, depending on their contribution to the LNB saturation and then applying a different back-off factors to each group of BSs. Since the maximum EIRP per BS is 31 dBW/5MHz, we fixed the back-off levels to be between 10 and 31 dB, in a steps of 5 dB. The lowest back-off level was fixed to 10 dB because, after some testing, it was find out that lower back-off values did not make a significant impact unless a huge number of BS were concerned with this back-off level. Next, we have ordered the BSs according to its contribution to the LNB saturation and segmented the BSs into different blocks. The main design intuition behind this segmentation was to have a balanced number of BSs within each segment. Following this design approach, the following clusters have been defined:

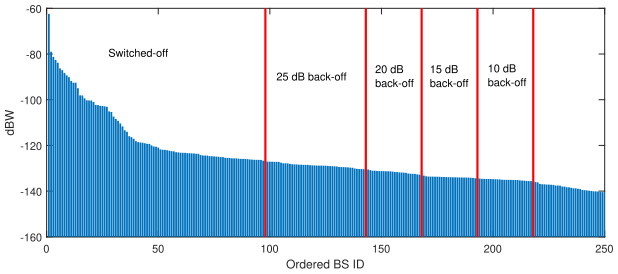

FIGURE 13. BSs segmentation for the power back-off strategy assuming antenna type 2 and margin of 25 dB.

- **Switch-off group**: BSs generating >-127 dBW interference power
- **Group applying power back-off of** 25 **dB**: BSs generating between -130.5 dBW and -127 dBW interference power
- **Group applying power back-off of** 20 **dB**: BSs generating between -133.2 dBW and -130.5 dBW interference power
- **Group applying power back-off of** 15 **dB**: BSs generating between -134.5 dBW and -133.2 dBW interference power
- **Group applying power back-off of** 10 **dB**: BSs generating between -136 dBW and -134.5 dBW interference power

The proposed segmentation and power back-off levels are illustrated in Fig. 13.

Following the suggested power back-off strategy, the aggregated interference seen at the LNB is -119.02 dBW, which is below the LNB threshold and, therefore, the LNB is not saturated. The number of BSs that need to be switched off completely reduced to 98 (with respect to the 202 obtained in Table 6). The price to pay for this reduction is the number of BSs that need to back-off power, which are 45, 25, 25 and 25 corresponding to the power back-off of 25 dB, 20 dB, 15 dB and 10 dB, respectively. In particular, a total of 218 BSs are affected by the power back-off strategy. The results have been summarized in Table 7 and the affected BSs are illustrated in Fig. 14.

Note that the LNB saturation criteria (i.e. -118 dBW interference threshold over the whole 3.4-3.8 GHz band) is much more restrictive than the interference protection criteria (i.e. -146.3871 dBW over 3.625-2.8 GHz band). This means that the mitigation strategies proposed in this Section to avoid the LNB saturation will comply as well with the interference protection criteria.

2) RESULTS WITH LNB MARGIN OF 10 dB

Assuming a 10 dB margin, the LNB interference saturation threshold is -73 dBm (or equivalently -103 dBW). As seen in the previous section, the total aggregated interference is equal to -62.15 dBW, which is still above the LNB saturation threshold. As a consequence, some kind of interference mitigation strategy has to be applied.

TABLE 7. Power back-off strategy results to avoid the LNB saturation (margin 25 dB).

Back-off factor	Number of BS affected	Percentage of BS switched off
Complete Switch-off	98	8.63%
25 **dB**	45	3.97%
20 **dB**	25	2.20%
15 **dB**	25	2.20%
10 **dB**	25	2.20%
Total	218	19.21%

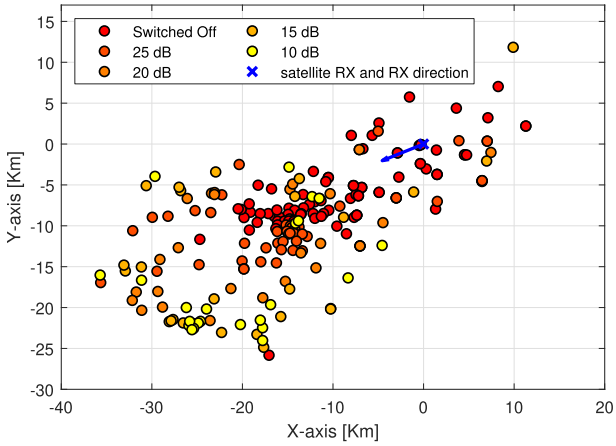

FIGURE 14. Location of BSs required to back-off power in order to not saturate the satellite LNB receiver assuming antenna type 2 and margin 25 dB.

TABLE 8. Switch-Off strategy results to avoid the LNB saturation (margin 10 dB).

Operator	Number of BS switched off	Percentage of BS switched off
1	17	3.78%
2	1	0.27%
3	18	5.71%
Total	36	3.17%

a: SWITCHING-OFF CRITICAL BS STRATEGY

Next, we apply the switching-off strategy and the results are summarized in Table 8. In particular, 36 BSs need to be switched off in total, representing a 3.17% of the total, and its location on the map are provided in Fig. 15 (note that we kept the same scale as in Fig. 12 for comparison purposes). As before, the most harmful BSs are located in close vicinity to the FSS Earth station receiver but the critical distance has been reduced from the $\sim$40 Km obtained with a 25 dB margin, to $\sim$14 Km with a 10 dB margin.

b: BS POWER BACK-OFF STRATEGY

Finally, we evaluate the alternative solution based on a power back-off strategy. Following a similar design approach as in Section III-C.1, the following clusters have been defined:

- **Switch-off group**: BSs generating >-93 dBW interference power
- **Group applying power back-off of** 25 **dB**: BSs generating between -100.5 dBW and -93 dBW interference power

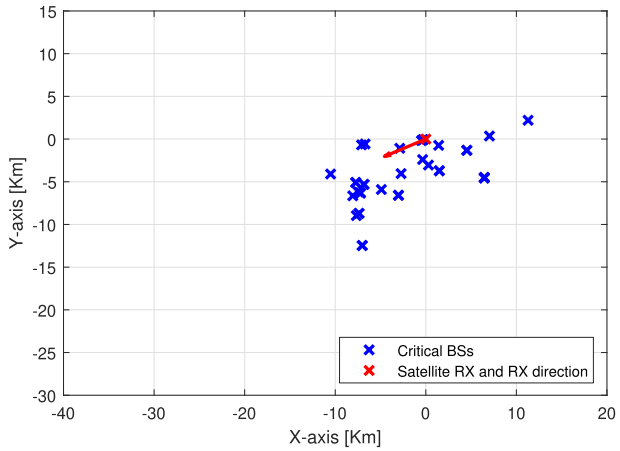

FIGURE 15. Location of BSs required to be switched off in order to not saturate the satellite LNB receiver assuming antenna type 2 and margin of 10 dB.

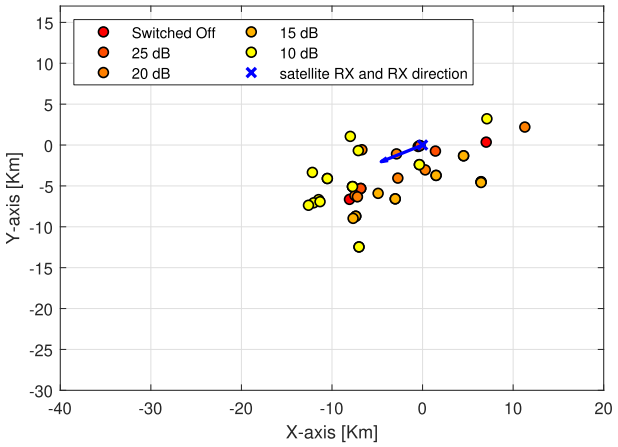

FIGURE 16. Location of BSs required to back-off power in order to not saturate the satellite LNB receiver assuming antenna type 2 and margin 10 dB.

TABLE 9. Power back-off strategy results to avoid the LNB saturation (margin 10 dB).

Back-off factor	Number of BS affected	Percentage of BS switched off
Complete Switch-off	13	1.15%
25 **dB**	7	0.62%
20 **dB**	7	0.62%
15 **dB**	7	0.62%
10 **dB**	12	0.67%
Total	46	4.05%

- **Group applying power back-off of** 20 **dB**: BSs generating between −104 dBW and −100.5 dBW interference power
- **Group applying power back-off of** 15 **dB**: BSs generating between −112 dBW and −104 dBW interference power
- **Group applying power back-off of** 10 **dB**: BSs generating between −119.5 dBW and −112 dBW interference power

Following the suggested power back-off strategy, the aggregated interference seen at the LNB is −103.4 dBW, which is below the LNB threshold and, therefore, the LNB is not saturated. The number of BSs that need to be switched off completely reduced to 13 (with respect to the 36 obtained in Table 8). The price to pay for this reduction is the number of BSs that need to back-off power, which are 7, 7, 7 and 12 corresponding to the power back-off of 25 dB, 20 dB, 15 dB and 10 dB, respectively. In particular, a total of 46 BSs are affected by the power back-off strategy. The results have been summarized in Table 9 and the affected BSs are illustrated in Fig. 16, where the same scale as in Fig. 14 is maintained for comparison purposes. Clearly, the reduction of the LNB margin relaxes the saturation threshold resulting in a reduced number of affected BSs.

D. GENERALIZATION OF SATELLITE FILTER CUT-OFF FREQUENCY

In this section, we provide the mathematical close form expression of the satellite receiver filter as a function of the cut-off frequency f_{sat}. We use the latter expression to compute the maximum allowable interference values so that the satellite receiver is not saturated.

TABLE 10. LNB Threshold per operator.

Number of Operators	LNB Threshold per operator
3	-122.77 dBW
4	-124.02 dBW

TABLE 11. Maximum allowable interference per operator [3 operators].

Operator	f [MHz]	L(f) [dB]	Max. allowable interference [dBW]
1	3480	-37.02	-85.75
2	3550	-15.57	-107.20
3	3620	-0.25	-122.52

Assuming that the satellite filter is known and given by the curve illustrate in Fig. 5, we propose the following mathematical expression to account for the filter attenuation:

$$L(f) = \begin{cases} 0.3064\,(f - f_{\text{sat}}) - 0.25 & \text{if } 3400 \leq f < f_{\text{sat}}, \\ -0.25 & \text{if } f \geq f_{\text{sat}}\,. \end{cases} \quad (3)$$

In Table 10, we provide the LNB threshold per operator depending on the number of active operators. This is achieved by simply dividing the −118 dBW (assuming margin of 25dB) into the total number of operators.

Assuming 3 operators and the 3 × 70 MHz allocation, and $f_{\text{sat}} = 3600$ MHz, Table 11 shows the maximum allowable interference per operator. Note that these values would correspond to a fair interference reduction from each operator, meaning that each operator is forced to generate −122.77 dBW of interference at the satellite receiver.

E. USE OF ACTIVE ANTENNA SYSTEMS IN 5G

In this section, we investigate the advantage of Active Antenna Systems (AAS) on the considered coexistence scenario by assuming each BS equipped with an antenna array system. Mainly, the objective here is to utilize the AAS at the

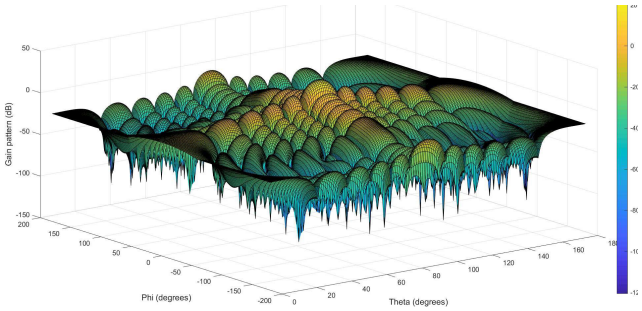

FIGURE 17. 3D composite radiation pattern of an active antenna.

TABLE 12. List of parameters used in AAS analysis.

Parameter	Value
Horizontal element spacing (d_H)	0.7λ
Vertical element spacing (d_V)	0.7λ
Downward tilting angle w.r.t. boresight (θ_{etilt})	$0°$
Horizontal scan angle w.r.t. boresight (ϕ_{escan})	$0°$
3 dB elevation beamwidth ($\theta_{3\text{dB}}$)	$65°$
3 dB azimuth beamwidth ($\phi_{3\text{dB}}$)	$65°$
No of elements in a vertical row (N_V)	8
No of elements in a horizontal row (N_H)	8
Side-lobe ratio	30 dB
Front-to back ratio	30 dB
Carrier frequency	3.4 GHz
Maximum element gain	8 dB
Correlation (ρ)	1

5G BSs to enable the steering of the main beam towards the 5G terminals so that the interference received at the FSS Earth station receiver will be minimized.

For modeling an AAS, we consider a planar Uniform Rectangular Array (URA) antenna with ($N_V \times N_H$) elements placed along the vertical and horizontal axes, respectively. The composite radiation pattern of such AAS is computed by the expressions provided in Table 5.4.4.2-3 of 3GPP TR 37.840 [34]. Fig. 17 illustrates the 3D pattern of the AAS obtained by utilizing the parameters listed in Table 12. It can be observed that a maximum gain of 26.06 dBi is achieved at the angular point of $\theta = 90°$ and $\phi = 0°$.

For the AAS impact study, we selected 5 BSs out from the most critical BSs identified in Fig. 23. The selected BSs' locations are illustrated in Fig. 18. We assume the worst-case scenario where the BS array antenna is mechanically steered towards the FSS Earth station receiver, as illustrated in Fig. 19. Next, we define a limited area where we randomly locate User Terminals (UTs). For this, we define a semi-circular area on the X-Y plane of radius 3 Km and 20° from the X-axis, as depicted in Fig. 19. We drop 100 UTs randomly over this defined area (an example of UTs distribution is shown in Fig. 20 for illustration purposes). For each UT, we point the AAS main beam toward that UT and evaluate the residual interference power received at the FSS Earth station receiver.

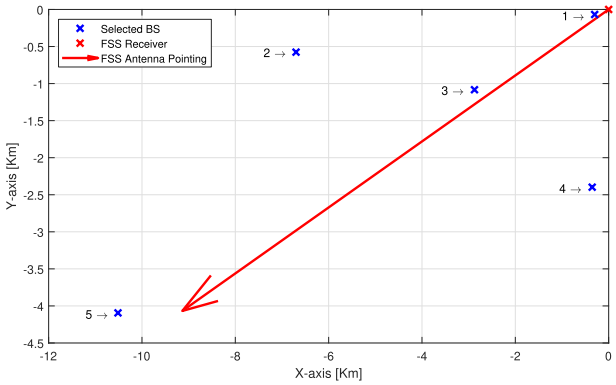

FIGURE 18. Location of selected BSs for the AAS impact study.

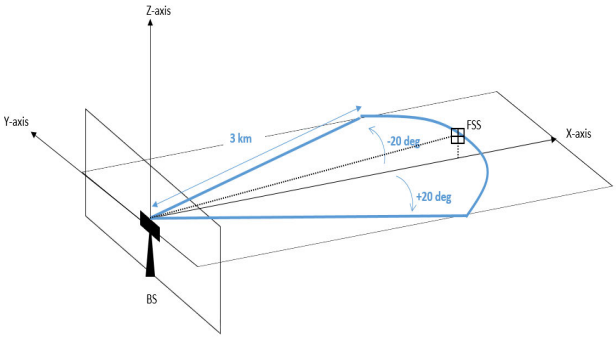

FIGURE 19. Scheme of the evaluation scenario for AAS.

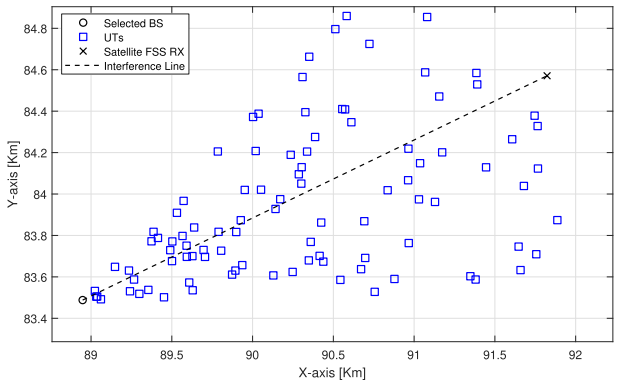

FIGURE 20. Example of 100 UTs random distribution.

While all the selected BSs depicted in Fig. 18 were saturating the LNB with the assumption of omni-directional antennas installed in the BSs, we can observe from Table 13 that the deployment of AAS tends to reduce the interference received at the FSS Earth station receiver by directive beam steering towards the UT locations. In particular, the last column of Table 13 provides the percentage of the 100 UTs under test that do not cause LNB saturation when AAS is implemented. From the 5 BSs analyzed, we have observed a significant reduction on the interference seen from the FSS Earth station receiver, which however sometimes is not enough to avoid the LNB saturation. For instance, in BS ID 1, which is located just a few meters from the FSS Earth station receiver and just

TABLE 13. AAS impact on the LNB saturation.

BS ID	Distance from FSS [Km]	ϕ angle [deg]	% of UTs that do not saturate the LNB
1	0.309	11.25	0%
2	6.724	19.09	31%
3	3.072	3.36	22%
4	2.424	57.62	20%
5	11.284	2.73	19%

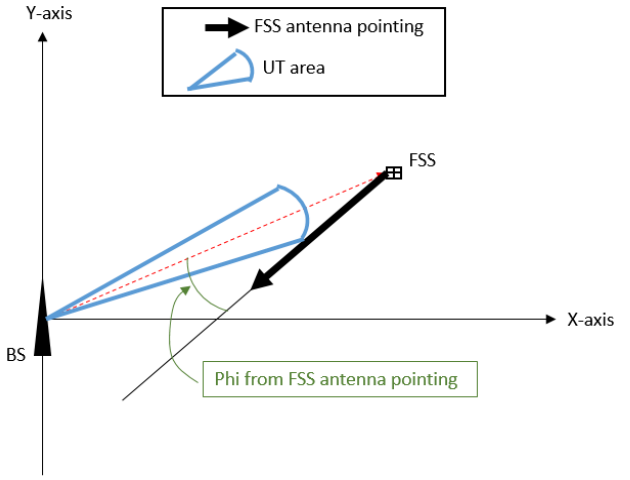

FIGURE 21. Illustration of the angle ϕ.

11.25 degrees off the FSS antenna pointing (a location very adverse from the point of view of interference), the reduction achieved with AAS is not enough to avoid the LNB saturation. For the rest of the BSs under study, we have achieved a reduction on the cases where the LNB is saturated of around 20% − 30%. This value strongly depends on the distance BS-FSS and the BS location with respect to the FSS antenna pointing. The later has been measured in Table 13 with the angle ϕ, whose geometry is illustrated in Fig. 21.

IV. 5G UPLINK SCENARIO

In this section, we evaluate the spectrum coexistence of FSS Earth station receivers and the 5G cellular uplink, i.e. User Terminals (UTs) transmitting towards the corresponding BS.

According to the results obtained for the downlink case in Sec. III, the frequency range of 3.410-3.620 GHz is identified as a potential band for 5G deployment, corresponding to the 70 MHz assignment option in Table 1, and illustrated in Fig. 2. Therefore, the study of the 5G uplink will be focused on this scenario.

In this section, we are interested in studying the impact of the interference generated by the transmissions of the UTs to the associated BS during their uplink mode in a satellite receiver located to a specific point on the ground with the view to receive data from a satellite during its downlink operation. As in the 5G downlink case, we assume the satellite receiver to operate in the area of 3.625 GHz and above and to employ the filter described in Section II-D, that nulls-out any interfering signal below 3.6 GHz. The interference model described in Section II-B is considered together with the specifications provided below.

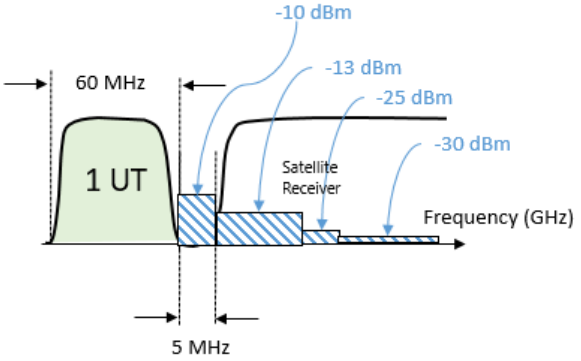

FIGURE 22. OOB emissions for a single UT in 60MHz bandwidth channels.

For the 5G uplink, the transmitters are the UTs. The UT Equivalent Isotropic Radiated Power (EIRP) is assumed to be 23 dBm/20 MHz (or −7 dBW/20 MHz). Note that, although usually 5G uplink employs power control techniques, in this work we assume the worst case scenario where all the users are employing their maximum transmission power. The UT height is assumed to be 4 meters (accounting for the worst case, i.e. vehicles). The UTs can be located anywhere on the territory provided that there is a nearby BS with 5G.

Regarding the OOB emissions, we model them based on the spectrum emission mask provided in 3GPP TS 38.101 Table 6.5.2.2-1 [35]. There, the OOB emissions are shown in each spectrum area based on its distance to the spectrum area occupied by a UT for its uplink transmission. For convenience, an example of spectrum emission mask of a single UT operating in a 60 MHz block adjacent to the FSS Earth station receiver is depicted on Fig. 22. In particular, based on the Table 6.5.2.2-1 in [35], for one active UT on the uplink, the satellite receiver will observe -13dBm from 3.625 GHz until 3.685 GHz (i.e. for 12 blocks of 5 MHz), −25 dBm for the next block of 5 MHz, and −30 dBm for the 23 remaining blocks of 5 MHz. In case that we have multiple active UTs that are operating on the same 60 MHz band, all of them will produce the same amount of OOB and will sum-up their contribution. The latter emissions are calculated based on the spurious emission model which is used for frequencies that are more than approximately 60 MHz apart from the occupied spectrum in place of the Table 6.5.2.2-1 in [35].

V. 5G UPLINK RESULTS

In this section, we present the results for the 5G cellular uplink scenario. This section is constituted by two subsections. In the first one, we examine only the impact of the OOB emissions to the the satellite receiver while in the second, the impact of the co-channel interference is taken into account as well.

A. IMPACT OF OOB EMISSIONS

In this section, we evaluate the impact of the OOB emissions for the 5G uplink scenario. The OOB of the operator allocated closer to the satellite spectrum are modeled as in Fig. 22,

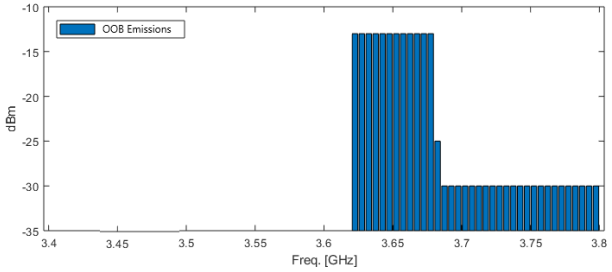

FIGURE 23. Interference due to the OOB emissions for a single UT using the closest 60 MHz block to the band of the satellite receiver.

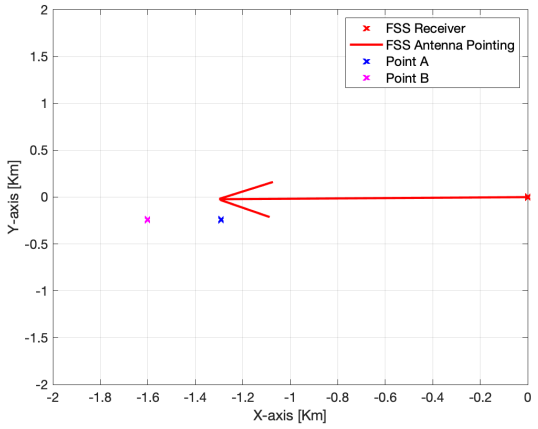

FIGURE 24. Scenario for 5G uplink OOB impact evaluation.

while the OBB of the other two operators is less critical, accounting for −30 dBm only. All in all, the strongest interference due to OOB emissions are due to the UTs associated with the operator that is located closer to the spectrum employed by the satellite receiver. The rest UTs associated with the other two operators are generating lower interference due to the OOB emissions that can be modeled by the constant value of −30 dBm. Having the aforementioned in mind, the resulting interference due to the OOB emissions is illustrated in Fig. 23 under the assumption that only a single user is active on the 60 MHz chunk closest to the band used by the satellite receiver. Note that the dominant value in this example is the −13 dBm generated by the first block of OOB within the satellite receiver band.

We now analyze the impact of the OOB emissions of the 5G uplink assuming that the UTs are located in two locations nearby to the satellite receiver. The first point, named as point A has altitude 239 meters and it is located in 1.29 Kms distance to the satellite receiver. The second point, namely point B, is placed on a position with altitude of 243 meters and it is located 1.6 Km apart from the satellite receiver. Both point A and B are illustrated in Fig. 24, together with satellite antenna dish pointing. The results have been obtained assuming the satellite receiver antenna type 1 (Section II-D).

For evaluating the effect of individual and aggregated interference at the satellite receiver, we again consider the interference protection criteria of I/N = −10 dB [31]. The

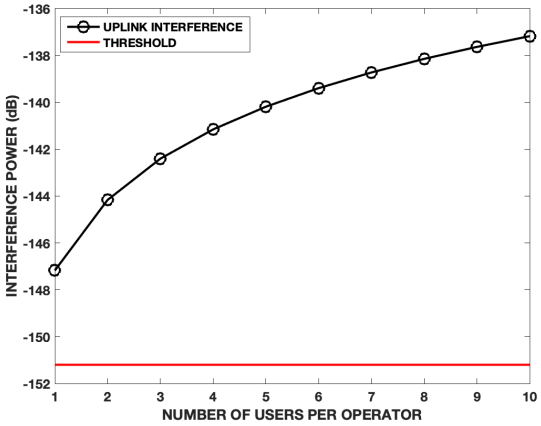

FIGURE 25. Interference Power Level vs Number of Users at the point A for the D = 12m 181/33 degrees Antenna (Antenna 1) - Only OOB.

noise level is calculated as in Section II-D and set to the value −141.20 dBW.

In the following, for both the selected locations, we will analyze two different cases:

- Fixing the location of the UTs, we will analyze how many UTs have to transmit simultaneously such that the aggregation of the OOB emissions at satellite side is above the threshold of -151.20 dBW.
- Assuming a single UT, we will analyze the distance from UT to the satellite receiver that causes OOB emissions on it above the threshold of -151.20 dBW.

Initially, we will examine the impact of the number of UTs required so that the aggregated OOB emissions caused harmful interference at satellite point. To that end, we will assume that each operator is allocating each time its complete spectrum (i.e. 60 MHz bandwidth channel) to a number of K users simultaneously. We will not consider any coordination among the users and it is assumed that they are capable of establishing their communication links by transmitting at full power simultaneously. Then, the total interference power due to the OOB emissions is aggregated. The interference model based on the OOB emissions for the uplink case is calculated as described in Section IV of the present paper. Note that the values of Table 6.5.2.2-1 [35] are converted for the 5 MHz bandwidth case considered here. In Figs. 25-26, the interference power due to the OOB emissions is calculated for the point A and the point B, respectively and plotted with respect the number of active users per operator. As it is shown for both points, the OOB emissions of even a single user per operator are enough to result in an interference power that is above the specified noise level threshold.

Next, we will consider a single UT and examine the impact of the distance from the FSS receiver. In particular, we will identify at which distance do the OOB emissions become critical for the satellite receiver. To that end, we start from the selected points A and B and move towards the FSS receiver by moving onto the line connecting the two ends. The propagation model and the OOB emissions are calculated as described in Section IV of the present paper.

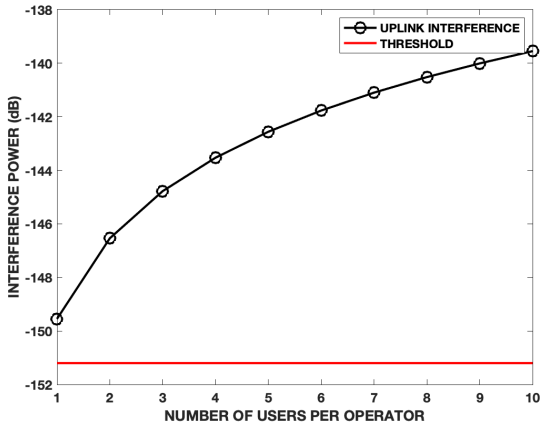

FIGURE 26. Interference Power Level vs Number of Users at the point B for the D = 12m 181/33 degrees Antenna (Antenna 1) - Only OOB.

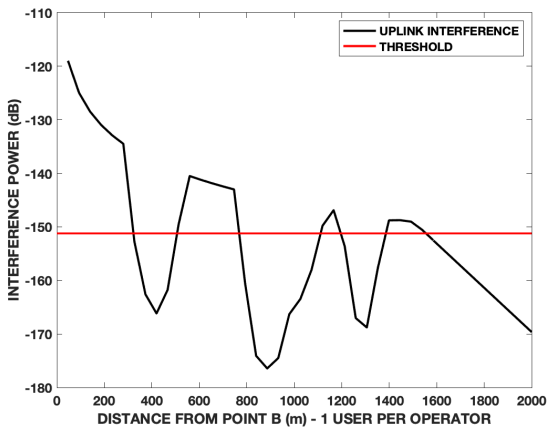

FIGURE 28. Interference Power Level vs Distance at the point B for the D = 12m 181/33 degrees Antenna (Antenna 1) - Only OOB.

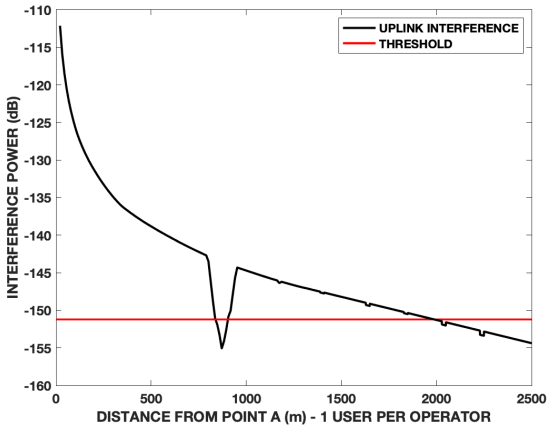

FIGURE 27. Interference Power Level vs Distance at the point A for the D = 12m 181/33 degrees Antenna (Antenna 1) - Only OOB.

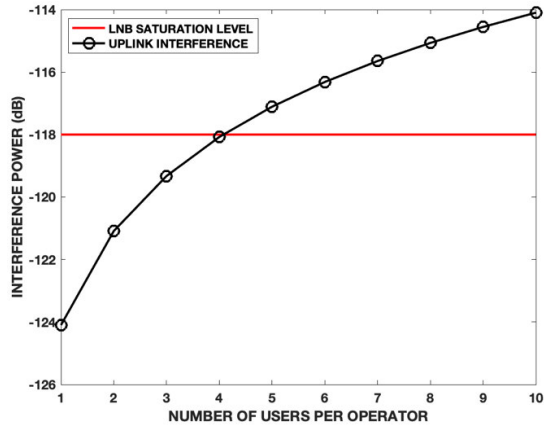

FIGURE 29. Interference Power Level vs Number of Users at the point A for the D = 12m 181/33 degrees Antenna (Antenna 1) - Only OOB.

In Figs. 27-28, the interference power due to the OOB emissions is calculated for the two considered points, respectively and plotted with respect to the distance to the FSS receiver. As it is shown, for the case of point A, the threshold is exceeded when the distance to the satellite terminal point is at around 2000 meters, although around 800 meters there is a short interval where the received interference due to the OOB emissions becomes again not harmful. This is probably due to the terrain variations, which affect the propagation loss and the received power at satellite receiver. Regarding the case of point B, the UT does not create harmful interference until it reaches a distance of about 1600 meters from the point of the satellite receiver. Large variations of the interference level are observed in the present case, which can be attributed as well to the corresponding variations on the terrain. In general, and as expected, for both cases, the interference is increasing as we come closer to the point of the satellite receiver.

B. IMPACT OF CO-CHANNEL INTERFERENCE ON THE FSS EARTH STATION RECEIVER LNB SATURATION

In this section, we calculate the impact of the uplink transmissions in the LNB considering the two selected points of Section V-A. In the present study, both the interference due to co-channel transmissions and OOB emissions is considered. Note that, as also analyzed on Section III, LNB is considered saturated when the total interference is above −118dB for a margin of 25dB.

As before, we divide the study of the LNB saturation into two cases:

- Fixing the location of the UTs, we will analyze how many UTs have to transmit simultaneously such that the aggregation of the interference at the point of the satellite receiver is above the LNB saturation threshold
- Assuming a single UT, we will analyze the distance from UT to the point of the satellite receiver that causes interference at the FSS Earth station receiver above the LNB saturation threshold.

Herein, we examine the impact of the number of UTs required to saturate the LNB of satellite receiver's antenna. To that end, we assume that each operator is allocating its whole spectrum of 60 MHz bandwidth to a number of UTs simultaneously. As for the OOB emissions only case (Section V-A), UT coordination is assumed to allow

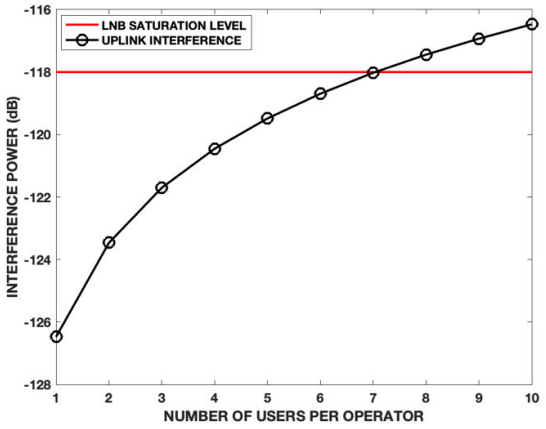

FIGURE 30. Interference Power Level vs Number of Users at the point B for the D = 12m 181/33 degrees Antenna (Antenna 1) - Only OOB.

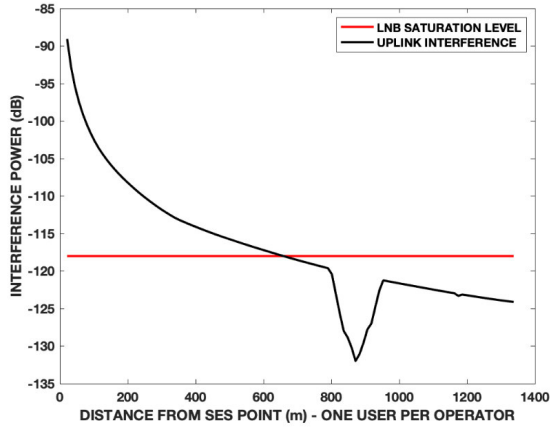

FIGURE 31. Interference Power Level vs Distance at the point A for the D = 12m 181/33 degrees Antenna (Antenna 1) - Only OOB.

coexistence in the same band. As before, the OOB emissions and the propagation model are computed following Section V.

Figs. 29-30 show the results for point A and point B, respectively. In the aforementioned figures, the aggregated interference seen at the satellite receiver's side versus the number of UTs per operator that are simultaneously active is depicted. As it is shown, for point A, only 4 UTs are enough so that the aggregated interference saturates the LNB. On the other hand, the LNB is saturated for 7 UTs for point B. Thus, for both cases we can conclude that there is space for some users without leading the LNB to saturation. We close this section, by examining the impact of the distance of a single UT from the FSS Earth station receiver in terms of the LNB saturation. To that end, we start from the selected points A and B and move towards the FSS Earth station receiver by moving onto the line that are connecting the end points. The aim is to check at which distance from the FSS point of interest the LNB is saturated. The rest of the calculations are done as described on Section V-A for the OOB emissions only case.

Figs. 31-32 illustrate the aggregated interference generated from a single UT and observed at the satellite receiver's side

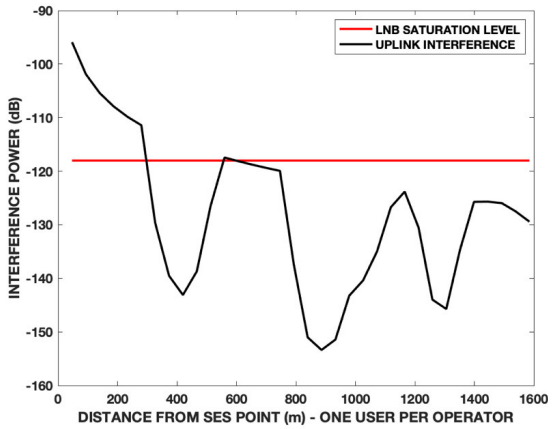

FIGURE 32. Interference Power Level vs Distance at the point B for the D = 12m 181/33 degrees Antenna (Antenna 1) - Only OOB.

for the both the examined points and plotted with respect to the distance to the FSS Earth station receiver. For the case of point A, the LNB is saturated when we reach a distance of 600m to the satellite receiver's location. For the case of point B, the distance is reduced to 550 meters and thus, the terminal can be closer compared to the former case.

VI. CONCLUSION

This paper addresses the potential C-band spectrum coexistence between the forthcoming 5G cellular systems and a FSS Earth station receiver. We first evaluated the impact of the 5G downlink for individual BSs and we found out that the OOB of BSs located at close vicinity of the satellite receiver, i.e. 16 Km, can perturb the satellite receiver operation, even when they are not aligned with the satellite antenna pointing. We performed the same exercise assuming co-channel interference of the individual BSs to the FSS Earth station receiver and it was observed that the percentage of critical BSs increases, as the maximum separation distance between BS and FSS Earth station receiver is of 16 Km if they are not aligned to the satellite receiver antenna pointing, while this maximum distance increases up to 40 Km when the BS locations are aligned with the satellite antenna pointing. Next, we evaluated the aggregated interference caused by a group of BSs belonging to the same operator for different frequency allocations (i.e. overlapping and non-overlapping with the satellite system). In this case, we observe that the operator assigned the frequency block adjacent to the 3.625 GHz limit is the one causing harmful interference to the FSS Earth station receiver. We showed how this interference can be relaxed by switching off those BSs located near to the FSS Earth station receiver. Finally, the impact of aggregated interference was studied with respect to the LNB saturation point, and we concluded that interference avoidance techniques need to be applied to avoid the LNB saturation, even when the 5G cellular downlink does not overlap with the satellite system. Furthermore, it has been observed that AAS can help in reducing the interference received at the FSS Earth station receiver by directive beam steering towards the UT locations.

Regarding the 5G uplink study, we observed that the OOB emissions are critical, since only 1 UT can already generate harmful interference to the FSS Earth station receiver side when they are located at a distance of 1Km from it. Regarding the aggregated co-channel interference, we showed that the LNB can be saturated with 4 simultaneous active UTs. Obviously, the distance between the FSS Earth station receiver and the UTs has a strong effect. The closer the UT to the FSS Earth station receiver, the higher the interference. In certain directions, the OOB emissions of a single UT become harmful at 1 Km distance, and the aggregated interference of a single UT saturates the LNB at 550 m distance.

REFERENCES

[1] A. Osseiran, F. Boccardi, V. Braun, K. Kusume, P. Marsch, M. Maternia, O. Queseth, M. Schellmann, H. Schotten, H. Taoka, H. Tullberg, M. A. Uusitalo, B. Timus, and M. Fallgren, "Scenarios for 5G mobile and wireless communications: The vision of the METIS project," *IEEE Commun. Mag.*, vol. 52, no. 5, pp. 26–35, May 2014.

[2] S. Mumtaz, A. Jamalipour, H. Gacanin, A. Rayes, M. I. Ashraf, R. Ting, and D. Zhang, "Licensed and unlicensed spectrum for future 5G/B5G wireless networks," *IEEE Netw.*, vol. 33, no. 4, pp. 6–8, Jul. 2019.

[3] M. Matinmikko-Blue, S. Yrjola, V. Seppanen, P. Ahokangas, H. Hammainen, and M. Latva-Aho, "Analysis of spectrum valuation elements for local 5G networks: Case study of 3.5-GHz band," *IEEE Trans. Cognit. Commun. Netw.*, vol. 5, no. 3, pp. 741–753, Sep. 2019.

[4] G. Hattab and M. Ibnkahla, "Multiband spectrum access: Great promises for future cognitive radio networks," *Proc. IEEE*, vol. 102, no. 3, pp. 282–306, Mar. 2014.

[5] S. K. Sharma, T. E. Bogale, L. B. Le, S. Chatzinotas, X. Wang, and B. Ottersten, "Dynamic spectrum sharing in 5G wireless networks with full-duplex technology: Recent advances and research challenges," *IEEE Commun. Surveys Tuts.*, vol. 20, no. 1, pp. 674–707, 1st Quart., 2018.

[6] E. Lagunas, S. K. Sharma, S. Maleki, S. Chatzinotas, and B. Ottersten, "Resource allocation for cognitive satellite communications with incumbent terrestrial networks," *IEEE Trans. Cognit. Commun. Netw.*, vol. 1, no. 3, pp. 305–317, Sep. 2015.

[7] Digital Europe. (Jan. 2018). *5G Spectrum Policy Recommendations*. Accessed: Mar. 10, 2020. [Online]. Available: http://www.digitaleurope.org/DesktopModules/Bring2mind/DMX/Download.aspx?Command=Core_Download&EntryId=2595&language=en-US&PortalId=0&TabId=353

[8] European Conference of Postal and Telecommunications Administrations (CEPT), Electronic Communications Committee (ECC). (Sep. 2017). *The Road to 5G Deployment*. Accessed: Mar. 10, 2020. [Online]. Available: http://apps.ero.dk/eccnews/sep-2017/index.html

[9] 5G Infrastructure Association (5G-PPP). (Jun. 2017). *The Need for 5G Spectrum*. Accessed: Mar. 10, 2020. [Online]. Available: https://5g-ppp.eu/wp-content/uploads/2017/03/2_EC_Stantchev_5G-WS_5GPPP_June7.pdf

[10] World Broadcasting Unions (WBU). (Sep. 2018). *WBU Position on C-Band*. Accessed: Mar. 10, 2020. [Online]. Available: https://worldbroadcastingunions.org/wbu-position-on-c-band/

[11] ITU-News. *WRC-19 Identifies Additional Frequency Bands for 5G*. Accessed: Mar. 10, 2020. [Online]. Available: https://news.itu.int/wrc-19-agrees-to-identify-new-frequency-bands-for-5g/

[12] Space-News. *Traction Building to Add C-Band to Next World Radiocommunication Conference Agenda*. Accessed: Mar. 10, 2020. [Online]. Available: https://spacenews.com/traction-building-to-add-c-band-to-next-world-radiocommunication-conference-agenda/

[13] ASIASAT. (Jun. 2018). *The Importance of Retaining C-Band for Satellite Service in the Asia–Pacific*. Accessed: Mar. 10, 2020. [Online]. Available: https://www.asiasat.com/sites/default/files/importance-of-retaining-cband-for-satellite-service-in-asia-pacific-region.pdf

[14] Netherlands Organisation for Applied Scientific Research (TNO). (Nov. 2018). *Co-Existence of 5G Mobile Networks With C-Band Satellite Interception in Burum*. Accessed: Mar. 10, 2020. [Online]. Available: https://www.kivi.nl/uploads/media/5c210b4f96aac/18310117+bijlage+1.pdf

[15] M. Kassem and M. Marina, "Future wireless spectrum below 6 GHz: A UK perspective," in *Proc. IEEE Int. Symp. Dyn. Spectr. Access Netw. (DySPAN)*, Stockholm, Sweden, Oct. 2015, pp. 59–70.

[16] L. Sastrawidjaja and M. Suryanegara, "Regulation challenges of 5G spectrum deployment at 3.5 GHz: The framework for indonesia," in *Proc. Electr. Power, Electron., Commun., Controls Informat. Seminar (EECCIS)*, Batu, Indonesia, Oct. 2018, pp. 213–217.

[17] C. Carciofi, P. Grazioso, V. Petrini, E. Spina, D. Massimi, G. De Sipio, E. Scognamiglio, V. Sorrentino, A. Casagni, L. Guoyue, Z. Lai, and R. Rudd, "Co-channel and adjacent-channel coexistence between LTE-TDD and VSAT DVB-S in C-band: Experimental campaign on consumer VSAT receivers," in *Proc. IEEE 29th Annu. Int. Symp. Pers., Indoor Mobile Radio Commun. (PIMRC)*, Bologna, Italy, Sep. 2018, pp. 1–5.

[18] W. A. Hassan, H.-S. Jo, and A. R. Tharek, "The feasibility of coexistence between 5G and existing services in the IMT-2020 candidate bands in malaysia," *IEEE Access*, vol. 5, pp. 14867–14888, 2017.

[19] C. V. R. Rodriguez, M. P. C. Almeida, C. E. O. Vargas, A. Tamo, and L. S. Mello, "Interference simulation between 5G and GSO–NGSO networks at 27-30 GHz range," in *Proc. IEEE-APS Top. Conf. Antennas Propag. Wireless Commun. (APWC)*, Granada, Spain, Sep. 2019, pp. 202–205.

[20] M. Shaat, A. I. Perez-Neira, G. Femenias, and F. Riera-Palou, "Joint frequency assignment and flow control for hybrid terrestrial-satellite backhauling networks," in *Proc. Int. Symp. Wireless Commun. Syst. (ISWCS)*, Bologna, Italy, Aug. 2017, pp. 293–298.

[21] S. Chatzinotas, B. Evans, A. Guidotti, V. Icolari, E. Lagunas, S. Maleki, S. K. Sharma, D. Tarchi, P. Thompson, and A. Vanelli-Coralli, "Cognitive approaches to enhance spectrum availability for satellite systems," *Int. J. Satell. Commun. Netw.*, vol. 35, no. 5, pp. 407–442, Sep. 2017.

[22] *Characteristics of Terrestrial IMT-Advanced Systems for Frequency Sharing/Interference Analyses*, document ITU-R M.2292-0, Dec. 2013. [Online]. Available: https://www.itu.int/dms_pub/itu-r/opb/rep/R-REP-M.2292-2014-PDF-E.pdf

[23] *IMT for 2020 and Beyond*. Accessed: Mar. 10, 2020. [Online]. Available: https://www.itu.int/en/ITU-R/study-groups/rsg5/rwp5d/imt-2020/Pages/default.aspx

[24] NOKIA. (Dec. 2016). *Nokia and Smart Showcase Live 5G for the First Time in the Philippines*. Accessed: Mar. 10, 2020. [Online]. Available: https://www.nokia.com/about-us/news/releases/2016/12/16/nokia-and-smart-showcase-live-5g-for-the-first-time-in-the-philippines/

[25] *Prediction Procedure for the Evaluation of Interference Between Stations on the Surface of the Earth at Frequencies Above About 0.1 GHz*, document ITU-R P.452-16, Jul. 2015.

[26] E. Lagunas, S. Sharma, S. Maleki, S. Chatzinotas, and B. Ottersten, "Impact of terrain aware interference modeling on the throughput of cognitive Ka-band satellite systems," in *Proc. Ka Broadband Commun. Conf. (KaConf)*, Bologna, Italy, Oct. 2015, pp. 1–8.

[27] ECC. (Jul. 2018). *Analysis of the Suitability of the Regulatory Technical Conditions for 5G MFCN Operation in the 3400-3800 MHz Band*. Accessed: Mar. 10, 2020. [Online]. Available: https://www.ecodocdb.dk/download/5ffb56c9-9c78/ECCRep281.pdf

[28] *Reference Radiation Pattern of Earth Station Antennas in the Fixed-Satellite Service for Use in Coordination and Interference Assessment in the Frequency Range From 2 to 31 GHz*, document ITU-R S.465-6 (01/2010), Jan. 2010.

[29] *Sharing Studies Between International Mobile Telecommunication-Advanced Systems and Geostationary Satellite Networks in the Fixed-Satellite Service in the 3 400-4 200 MHz and 4 500-4 800 MHz Frequency Bands in the WRC Study Cycle Leading to WRC-15*, document ITU-R S.2368-0, 2015.

[30] SatCom Services. (Jan. 2020). *Model 6.3m Cassegrain Antenna*. Accessed: Mar. 10, 2020. [Online]. Available: https://satcom-services.com/product/model-6-3m-cassegrain-antenna/

[31] S. Sharma, S. Maleki, S. Chatzinotas, J. Grotz, and B. Ottersten, "Implementation issues of cognitive radio techniques for Ka-band (17.7–19.7 GHz) SatComs," in *Proc. Adv. Satell. Multimedia Syst. Conf. 13th Signal Process. Space Commun. Workshop (SPSC)*, Livorno, Italy, 2014, pp. 241–248.

[32] Y. Zhou, Z. Zhao, Y. Louet, Q. Ying, R. Li, X. Zhou, X. Chen, and H. Zhang, "Large-scale spatial distribution identification of base stations in cellular networks," *IEEE Access*, vol. 3, pp. 2987–2999, 2015.

[33] Norsat International. *LNB C-Band*. Accessed: Mar. 10, 2020. [Online]. Available: https://products.norsat.com/UserFiles/NorsatDocs/3200N-BPF%20Spec%20She%et.pdf

[34] *Technical Specification Group Radio Access Network; Study of Radio Frequency (RF) and Electromagnetic Compatibility (EMC) Requirements for Active Antenna Array System (AAS) Base Station*, document 37.840 V12.1.0, 3GPP, Dec. 2013.
[35] *New WID on New Radio Technology*, document RP-170855, 3GPP, 3GPP RAN 75, Dubrovnik, Croatia, Mar. 2017. [Online]. Available: https://www.3gpp.org/release-15

EVA LAGUNAS (Senior Member, IEEE) received the M.Sc. and Ph.D. degrees in telecommunications engineering from the Polytechnic University of Catalonia (UPC), Barcelona, Spain, in 2010 and 2014, respectively. She was a Research Assistant with the Department of Signal Theory and Communications, UPC, from 2009 to 2013. In 2009, she was a Guest Research Assistant with the Department of Information Engineering, University of Pisa, Italy. From November 2011 to May 2012, she held a Visiting Research Appointment at the Center for Advanced Communications (CAC), Villanova University, PA, USA. In 2014, she joined the Interdisciplinary Centre for Security, Reliability, and Trust (SnT), University of Luxembourg, where she currently holds a Research Scientist position. Her research interests include radio resource management and general wireless networks optimization.

CHRISTOS G. TSINOS (Member, IEEE) received the Diploma degree in computer engineering and informatics, the M.Sc. and Ph.D. degrees in signal processing and communication systems, and the M.Sc. degree in applied mathematics from the University of Patras, Greece, in 2006, 2008, 2013, and 2014, respectively. From 2014 to 2015, he was a Postdoctoral Researcher with the University of Patras. In 2015, he joined the Interdisciplinary Centre for Security, Reliability, and Trust (SnT), University of Luxembourg, Luxembourg, where currently is a Research Scientist. In the past, he was involved in a number of different Research and Development projects funded by national and/or EU funds. He is currently the PI of Research and Development Project Energy and CompLexity EffiCienT mIllimeter-wave Large-Array Communications (ECLECTIC), funded under FNR CORE Framework. His current research interests include signal processing for mm-wave, massive MIMO, cognitive radio and satellite communications, and hyperspectral image processing. He is a member of the Technical Chamber of Greece.

SHREE KRISHNA SHARMA (Senior Member, IEEE) received the Ph.D. degree in wireless communications from the University of Luxembourg, in 2014. He is currently Research Scientist with the SnT, University of Luxembourg. Prior to this, he worked as a Postdoctoral Fellow with the University of Western Ontario, Canada, and a Research Associate at the SnT being involved in different European, national and ESA projects. His current research interests include 5G and beyond wireless, the Internet of Things, machine learning, edge computing and optimization of distributed communications, computing and caching resources. He has published about 100 technical articles in scholarly journals, international conferences and book chapters, and has over 2100 Google scholar citations. He has been a TPC Member for a number of international conferences, including the IEEE ICC, the IEEE GLOBECOM, the IEEE PIMRC, the IEEE VTC, and the IEEE ISWCS. He was a recipient of several prestigious awards including the 2018 EURASIP Best Journal Paper Award, the CROWNCOM 2015 Best Paper Award, and the FNR Award for Outstanding Ph.D. Thesis 2015. He has been serving as a Reviewer for several international journals and conferences, and an Associate Editor for IEEE Access journal. He co-organized a special session in the IEEE PIMRC 2017 and the workshop in the IEEE SECON 2019. He worked as a Track Co-Chair of the IEEE VTC-fall 2018 conference, and published an IET book on *Satellite Communications in the 5G Era* as a Lead Editor.

SYMEON CHATZINOTAS (Senior Member, IEEE) received the M.Eng. degree in telecommunications from the Aristotle University of Thessaloniki, Thessaloniki, Greece, in 2003, and the M.Sc. and Ph.D. degrees in electronic engineering from the University of Surrey, Surrey, U.K., in 2006 and 2009, respectively. He is currently a Full Professor, the Chief Scientist I, and the Co-Head of the SIGCOM Research Group, SnT, University of Luxembourg. In the past, he has been a Visiting Professor with the University of Parma, Italy. He was involved in numerous Research and Development projects for the National Center for Scientific Research Demokritos, the Center of Research and Technology Hellas, and the Center of Communication Systems Research, University of Surrey. He has (co)authored more than 400 technical articles in refereed international journals, conferences, and scientific books. He was a co-recipient of the 2014 IEEE Distinguished Contributions to Satellite Communications Award, the CROWNCOM 2015 Best Paper Award and the 2018 EURASIC JWCN Best Paper Award. He is currently in the editorial board of the IEEE Open Journal of Vehicular Technology and the *International Journal of Satellite Communications and Networking*.